

Article

Vibrational Properties and DFT Calculations of Perovskite-Type Methylhydrazinium Manganese Hypophosphite

Aneta Ciupa-Litwa ¹, Maciej Ptak ^{1,*}, Edyta Kucharska ², Jerzy Hanuza ¹ and Mirosław Maćzka ¹

¹ Institute of Low Temperature and Structure Research, Polish Academy of Sciences, 50-422 Wrocław, Poland; a.ciupa@intibs.pl (A.C.-L.); j.hanuza@intibs.pl (J.H.); m.maczka@intibs.pl (M.M.)

² Department of Bioorganic Chemistry, Faculty of Production Engineering, University of Economics and Business, 118/120 Komandorska str., 53-345 Wrocław, Poland; edyta.kucharska@ue.wroc.pl

* Correspondence: m.ptak@intibs.pl; Tel.: +48-71-3954-162

Academic Editors: Jürgen Köhler and Marco Anni

Received: 11 September 2020; Accepted: 5 November 2020; Published: 9 November 2020



Abstract: Recently discovered hybrid perovskites based on hypophosphite ligands are a promising class of compounds exhibiting unusual structural properties and providing opportunities for construction of novel functional materials. Here, we report for the first time the detailed studies of phonon properties of manganese hypophosphite templated with methylhydrazinium cations ($[\text{CH}_3\text{NH}_2\text{NH}_2][\text{Mn}(\text{H}_2\text{PO}_2)_3]$). Its room temperature vibrational spectra were recorded for both polycrystalline sample and a single crystal. The proposed assignment based on Density Functional Theory (DFT) calculations of the observed vibrational modes is also presented. It is worth noting this is first report on polarized Raman measurements in this class of hybrid perovskites.

Keywords: hypophosphite; methylhydrazinium cation; DFT; Raman; IR

1. Introduction

In recent years, a lot of attention has been devoted to hybrid organic-inorganic compounds of general formula ABX_3 (A = organic cation; B = divalent metal cation; X = halide, formate (HCOO^-), azide (N_3^-), cyanide (CN^-), dicyanamide ($\text{N}(\text{CN})_2^-$, dca^-), hypophosphite (H_2PO_2^-)), crystallizing in a perovskite-type architecture due to their interesting physicochemical properties including photovoltaic [1], light-emitting [2–5], multiferroic [6–8], barocaloric [9,10], and non-linear optical (NLO) [11–13] properties. The structure-related properties of these compounds depend on flexibility of ligands, size and shape of organic cations as well as their ability to form hydrogen bonds (HBs) with the anionic framework. In this respect, very large flexibility of the dca^- ligands and pronounced temperature-induced disorder of organic cations at elevated temperatures is responsible for unusual softness and promising barocaloric properties of dicyanamides [9,10,14,15]. Order-disorder phenomena are also responsible for onset of spontaneous polarization in formates and their multiferroic properties [6,8]. These phenomena can be tuned by proper use of organic cations and we showed for the first time in 2017 that methylhydrazinium cation ($\text{CH}_3\text{NH}_2\text{NH}_2^+$, MHy^+) may also be used for the construction of perovskite-type formates [8]. Very recently, we showed that MHy^+ also allows extending the formation of three-dimensional (3D) lead halides beyond two already known methylammonium and formamidinium analogues [12,13]. This cation also allows constructing the two-dimensional (2D) perovskite of the formula MHy_2PbI_4 [5] as well as 3D hypophosphite $[\text{MHy}][\text{Mn}(\text{H}_2\text{PO}_2)_3]$ [5].

While perovskite-type halides, formates, azides, cyanides, and dicyanamides have been known for a long time, their hypophosphite analogues were discovered for the first time in 2017 [16].

Except for one magnesium analogue [17], all known compounds contain manganese as divalent cation [5,16,18,19]. Literature data show that although H_2POO^- ligand has a very similar size to the formate ion, the hypophosphite frameworks show much higher flexibility than their formate counterparts [16,19]. As a result, hypophosphites have higher potential than formates for structural distortion, which results in the presence of unconventional tilts of MnO_6 octahedra and columnar shifts [16,19]. Furthermore, they often show pronounced off-centering of organic cations away from the cavity center [16,19].

Up until now, Raman and IR studies were reported for only one hypophosphite, i.e., formamidinium manganese hypophosphite [20]. Regarding methylhydrazinium compounds, we reported Raman and IR data for some formates and two halides (MHy_2PbI_4 and MHyPbBr_3). However, deep understanding of vibrational modes of MHy^+ cations is still lacking and vibrational properties of recently discovered $[\text{MHy}][\text{Mn}(\text{H}_2\text{PO}_2)_3]$ are not known. We decided, therefore, to analyze vibrational properties of $[\text{MHy}][\text{Mn}(\text{H}_2\text{PO}_2)_3]$ crystal and propose reliable assignment of vibrational bands by performing Density Functional Theory (DFT) calculations.

2. Experimental Section

2.1. Synthesis of Single Crystals

$[\text{MHy}][\text{Mn}(\text{H}_2\text{POO})_3]$ crystals were grown by slow evaporation at 50°C of solution prepared by dissolving 5 mmol of MnCO_3 (99.9%, Sigma-Aldrich, Saint Louis, MO, USA) and 10 mmol (0.53 mL) of methylhydrazine (98%, Sigma-Aldrich) in 6.46 mL of aqueous solution of hypophosphorous acid (50%, Sigma-Aldrich) (equivalent of 60 mmol of H_3PO_2). Further details can be found in our previous paper [5].

2.2. Materials and Methods

Polycrystalline IR spectra were measured using a Nicolet iS50 FT-IR spectrometer. The standard KBr pellet method was used for the mid-IR range ($4000\text{--}400\text{ cm}^{-1}$) and nujol mull on a polyethylene plate for the far-IR range ($600\text{--}100\text{ cm}^{-1}$). Raman spectrum of powdered crystals was measured using a Bruker FT100/S spectrometer (Billerica, MA, USA) with YAG:Nd laser excitation (1064 nm). Polarized and temperature-dependent Raman spectra were measured using a Renishaw InVia Raman spectrometer (Wotton-under-Edge, UK), equipped with confocal DM2500 Leica optical microscope, a thermoelectrically cooled CCD as a detector, and an Ar^+ ion laser operating at 488 nm. Spectral resolution of both Raman and IR spectra was set to be 2 cm^{-1} and temperature was controlled using Linkam THMS600 cryostat cell (Tadworth, UK), equipped with quartz windows.

2.3. Computational Details

The geometry optimization of the molecular structure of the MHy^+ cation (Figure 1) was performed with the use of Gaussian 03 program package [21]. All calculations were performed using density functional three-parameters hybrid (B3LYP) methods [22–24] with the 6-311G(2d,2p) [25,26] basis set. In the geometry optimization, the structural parameters from X-ray diffraction studies were taken as input data. The comparison of the calculated and experimental bond lengths and bond angles is presented in Table S1. Geometry optimization was followed by the calculations of vibrational frequencies. The calculated harmonic frequencies were scaled using scaling factors (0.96 and 0.98) to correct the evaluated wavenumbers for vibrational anharmonicity and deficiencies inherent to the used computational level. Anharmonic wavenumbers were also calculated using deperturbed vibrational second-order perturbation theory (DVPT2). To assign the calculated modes, the Chemcraft computer program was used [27]. The Potential Energy Distribution (PED) of the normal modes among the respective internal coordinates was calculated for studied compound using the BALGA [28] program.

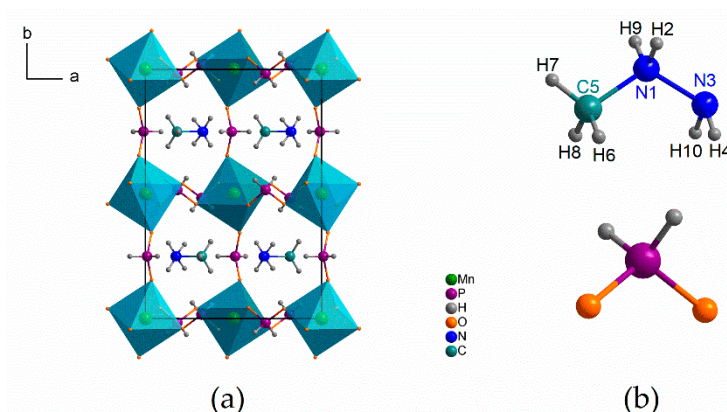


Figure 1. The crystal structure packing of $[\text{MHy}][\text{Mn}(\text{H}_2\text{POO})_3]$ taken from Ref. [5] (a) and the structural model of MHy^+ cation (with the atomic numbering used in the Density Functional Theory (DFT) calculations) and H_2POO^- anion (b).

3. Results and Discussion

3.1. Structure

As follows from Table S1, the calculated C-N and N-N bond lengths (1.506 and 1.447 Å, respectively) and C-N-N angle (118.3°) are in very good agreement with the experimental values (1.470, 1.442 Å and 116.3°, respectively [5]). The calculated C-H and N-H bonds are significantly longer than the experimental ones but it should be remembered that X-ray diffraction method is not sensitive for light atoms like hydrogen. The majority of the remaining calculated angles are also in agreement with the experimental ones.

3.2. Vibrational Properties

Experimental IR and Raman spectra of powdered crystals are presented in Figure 2, while polarized Raman spectra are depicted in Figure 3. Table 1 and Table S2 list the calculated and observed experimental wavenumbers as well as the proposed assignment.

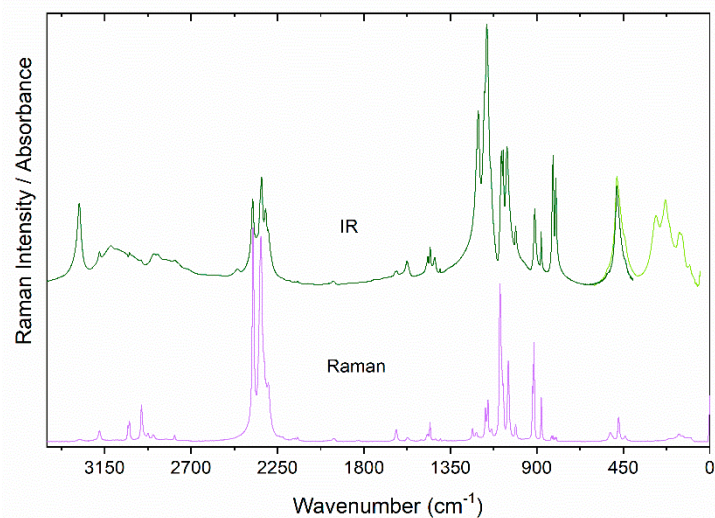


Figure 2. The polycrystalline IR and Raman spectra of the $[\text{MHy}][\text{Mn}(\text{H}_2\text{POO})_3]$ perovskite measured at room temperature.

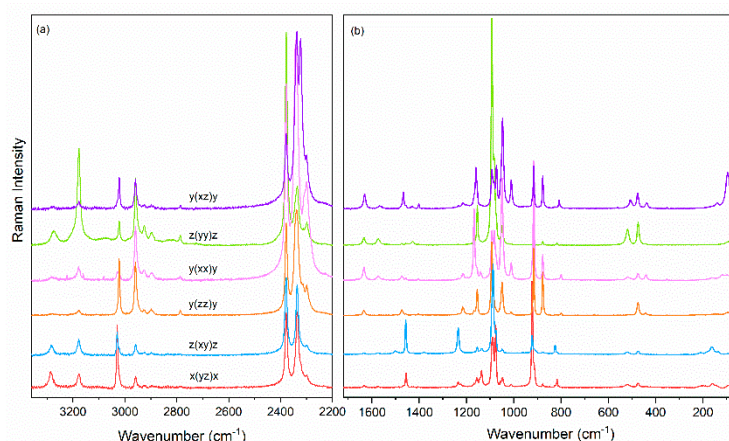


Figure 3. Polarized Raman spectra of the $[\text{MHy}][\text{Mn}(\text{H}_2\text{POO})_3]$ single crystal in the (a) $2200\text{--}3360\text{ cm}^{-1}$ and (b) $50\text{--}1720\text{ cm}^{-1}$ range.

Internal vibrations of MHy⁺ cation. Free MHy⁺ cation has 24 vibrational degrees of freedom that can be subdivided into symmetric stretching ($2\nu_s\text{NH}_2$), antisymmetric stretching ($2\nu_{as}\text{NH}_2$), scissoring ($2\delta\text{NH}_2$), rocking ($2\rho\text{NH}_2$), wagging ($2\omega\text{NH}_2$), and torsion or twisting ($2\tau\text{NH}_2$) modes of the NH_2 and NH_2^+ groups; symmetric stretching ($\nu_s\text{CNN}$), antisymmetric stretching ($\nu_{as}\text{CNN}$) and bending (δCNN) modes of the CNN skeletal group, and symmetric stretching ($\nu_s\text{CH}_3$), antisymmetric stretching ($2\nu_{as}\text{CH}_3$), symmetric bending ($\delta_s\text{CH}_3$), antisymmetric bending ($2\delta_{as}\text{CH}_3$), rocking ($2\rho\text{CH}_3$) and torsion (τCH_3) modes of the methyl group.

DFT calculations show that the N-H stretching modes of the terminal NH_2 (middle NH_2^+) groups are expected at $3388 + 3306\text{ cm}^{-1}$ ($3292 + 3289\text{ cm}^{-1}$) (Table 1). The former modes are observed in the experimental spectra as relatively narrow bands shifted to lower wavenumbers by $30\text{--}107\text{ cm}^{-1}$, compared to the calculated ones (Table 1 and Table S2). Small bandwidths and shifts are consistent with involvement of these NH_2 groups in formation of weak HBs (according to the X-ray diffraction, the $\text{N}\cdots\text{O}$ distance is 3.001 \AA [5]). It is worth noting that the 3281 cm^{-1} band is significantly weaker in the Raman spectrum than that observed at 3176 cm^{-1} , but opposite behavior is observed in the IR spectrum (Figure 2). Therefore, we assign the 3281 and 3176 cm^{-1} bands to antisymmetric and symmetric stretching, respectively. The modes calculated at $3292 + 3289\text{ cm}^{-1}$ are observed as broad and medium intensity IR bands at $3118 + 3085\text{ cm}^{-1}$ (Figure 2, Table S2). This behavior confirms involvement of the NH_2^+ groups in formation of medium strong HBs (the shortest $\text{N}\cdots\text{O}$ distance is 2.875 \AA [5]).

The C-H stretching modes of the methyl group are observed as the strongest Raman bands in the $3300\text{--}2700\text{ cm}^{-1}$ range. These bands are narrow and those at 3028 and 3021 cm^{-1} have significantly smaller intensity than that at 2958 cm^{-1} , allowing their assignment to antisymmetric and symmetric modes, respectively. Raman and IR spectra show also a few bands in the $2930\text{--}2700\text{ cm}^{-1}$ range that are not predicted by DFT calculations (Table 1 and Table S2). These bands correspond, therefore, to some combination modes.

The calculated scissoring modes of the NH_2 and NH_2^+ groups (1679 and 1607 cm^{-1} , respectively) are in good agreement with the observed ones (1632 and 1574 cm^{-1} , Table S2). Good agreement is also observed for the C-H bending modes that are predicted (observed) in the $1472\text{--}1439\text{ cm}^{-1}$ ($1474\text{--}1428\text{ cm}^{-1}$) range.

Table 1. Calculated (harmonic and anharmonic) wavenumbers for the MHy⁺ cation.

No.	ν_{harm}	ν_{harm}^1	ν_{anharm}	PED
1	3564	3421	3388	$\nu_{\text{as}}\text{NH}_2\text{-99}$
2	3477	3338	3306	$\nu_{\text{s}}\text{NH}_2\text{-100}$
3	3461	3323	3292	$\nu_{\text{as}}\text{NH}_2^+\text{-99}$
4	3425	3288	3289	$\nu_{\text{s}}\text{NH}_2^+\text{-98}$
5	3180	3053	3049	$\nu_{\text{as}}\text{CH}_3\text{-100}$
6	3166	3039	3029	$\nu_{\text{as}}\text{CH}_3\text{-100}$
7	3075	2952	3014	$\nu_{\text{s}}\text{CH}_3\text{-100}$
8	1700	1666	1679	$\delta\text{NH}_2\text{-80} + \delta\text{NH}_2^+\text{-20}$
9	1670	1637	1607	$\delta\text{NH}_2^+\text{-80} + \delta\text{NH}_2\text{-20}$
10	1499	1469	1472	$\delta_{\text{as}}\text{CH}_3\text{-91}$
11	1499	1469	1458	$\delta_{\text{as}}\text{CH}_3\text{-62} + \rho\text{NH}_2\text{-22} + \tau\text{NH}_2^+\text{-14}$
12	1490	1460	1449	$\tau\text{NH}_2^+\text{-38} + \delta_{\text{as}}\text{CH}_3\text{-35} + \rho\text{NH}_2\text{-26}$
13	1461	1432	1439	$\delta_{\text{s}}\text{CH}_3\text{-97}$
14	1443	1415	1401	$\omega\text{NH}_2^+\text{-86} + \delta_{\text{as}}\text{CH}_3\text{-15}$
15	1336	1309	1297	$\tau\text{NH}_2^+\text{-41} + \rho\text{CH}_3\text{-36} + \rho\text{NH}_2\text{-22}$
16	1219	1194	1176	$\rho\text{CH}_3\text{-50} + \omega\text{NH}_2\text{-25} + \nu\text{NH}_2^+\text{-NH}_2\text{-13} + \delta\text{NH}_2^+\text{-13}$
17	1117	1095	1091	$\rho\text{CH}_3\text{-42} + \rho\text{NH}_2\text{-25} + \tau\text{NH}_2^+\text{-32}$
18	1065	1043	1031	$\omega\text{NH}_2\text{-37} + \rho\text{CH}_3\text{-30} + \nu\text{NH}_2^+\text{-NH}_2\text{-20} + \nu\text{NH}_2^+\text{-CH}_3\text{-12}$
19	953	934	907	$\nu\text{NH}_2^+\text{-CH}_3\text{-48} + \omega\text{NH}_2\text{-27} + \nu\text{NH}_2^+\text{-NH}_2\text{-22}$
20	841	824	821	$\rho\text{NH}_2^+\text{-75} + \rho\text{CH}_3\text{-22}$
21	836	819	811	$\nu\text{NH}_2^+\text{-NH}_2\text{-46} + \nu\text{NH}_2^+\text{-CH}_3\text{-37} + \omega\text{NH}_2\text{-12}$
22	405	397	404	$\delta\text{CNN}\text{-87}$
23	281	275	252	$\tau\text{NH}_2\text{-73} + \tau\text{CH}_3\text{-27}$
24	225	220	245	$\tau\text{CH}_3\text{-73} + \tau\text{NH}_2\text{-27}$

¹ scaling factor = 0.98 (2499–0 cm⁻¹) + 0.96 (3500–2500 cm⁻¹); abbreviations: in-plane vibrations: ν —stretching; δ —bending; ρ —rocking; out-of-plane vibrations: ω —wagging; τ —twisting

According to the DFT calculations, τNH_2^+ , ωNH_2 , ωNH_2^+ , ρNH_2 and ρCH_3 modes should be observed in the 1449–1031 cm⁻¹ range. The mode calculated at 1031 cm⁻¹ cannot be observed in our spectra due to overlapping with strong bands of the hypophosphite ion. The remaining modes are, however, observed in the 1403–1136 cm⁻¹ range (Table S2).

In the 1020–770 cm⁻¹ range, three bands can be identified as arising from vibrations of MHy⁺ cation. The most intense Raman band at 878 cm⁻¹ can be unambiguously assigned to the $\nu_{\text{s}}\text{CNN}$ vibration calculated at 811 cm⁻¹. DFT predicts that the ρNH_2 mode should be observed at slightly higher wavenumber (821 cm⁻¹) than the $\nu_{\text{s}}\text{CNN}$ one. We locate, therefore, this mode in the 915–910 cm⁻¹ range. The band observed at 1010 cm⁻¹ (calculated at 907 cm⁻¹) can be assigned to the $\nu_{\text{as}}\text{CNN}$ mode.

DFT calculations predict the presence of three internal modes of MHy⁺ in the region below 500 cm⁻¹. We could identify two of these modes around 440 and 210 cm⁻¹ and assign them to δCNN and τCH_3 , respectively (Table 1 and Table S2).

Unit cell of $[\text{MHy}][\text{Mn}(\text{H}_2\text{PO}_2)_3]$ contains four MHy⁺ cations located at sites of C_s symmetry. Therefore, all internal modes of this cation should split into four components (see Table S3). Raman spectra clearly show that many A_g modes are observed at slightly different wavenumbers than their B_{1g}, B_{2g} or B_{3g} counterparts, i.e., the significant Davydov splitting is observed (Table S2). The largest differences are observed for the δNH_2^+ mode (1574 and 1568 cm⁻¹ for the A_g and B_{2g} mode, respectively) and $\delta_{\text{as}}\text{CH}_3$ mode (1451/1452 cm⁻¹ and 1457 cm⁻¹ for the A_g and B_{1g} mode, respectively). In other cases, the differences between wavenumbers of Raman components are less than 1–3 cm⁻¹. For instance, the symmetric stretching mode of the CH₃ group ($\nu_{\text{s}}\text{CH}_3$) is visible at 2959 cm⁻¹ for A_g and B_{2g} modes and at 2958 cm⁻¹ for B_{1g} and B_{3g} modes. Similar slight changes in the positions of Davydov components are observed for its antisymmetric counterpart ($\nu_{\text{as}}\text{CH}_3$), at 2959 cm⁻¹ for A_g and B_{2g} modes and at 2958 cm⁻¹ for B_{1g} and B_{3g} modes. It is worth mentioning that the size of Davydov splitting depends on the strength of intermolecular interactions occurring in the studied compound, namely, stronger interactions lead to larger Davydov splitting.

It is worth making a short comparison of the MHy^+ modes observed in this hypophosphite and related formate ($[\text{MHy}][\text{Mn}(\text{HCOO})_3]$) reported in the literature. According to the X-ray diffraction data, MHy^+ cations are ordered in the hypophosphite and the terminal NH_2 groups are involved in weak HBs, whereas in the formate these cations are disordered and the terminal groups form no HBs [5,8]. Furthermore, MHy^+ cation shifts away from the cavity center in the hypophosphite but sits in the center in the formate. This difference is related to more flexible P-O-Mn bindings compared to the C-O-Mn ones [5]. Raman and IR spectra reflect these differences very clearly. Firstly, stretching modes of the terminal NH_2 groups are shifted to higher wavenumbers for the formate (3317 and 3195 cm^{-1} [8]) due to lack of HBs interactions. The skeletal modes are, however, observed at very similar wavenumbers for the both analogues (the largest difference is only 3 cm^{-1}), reflecting similar geometry of MHy^+ cations. Secondly, stretching modes of the methyl groups in the formate are shifted up to 9 cm^{-1} due to larger constraint imposed on the MHy^+ cations. Thirdly, IR band corresponding to the ρNH_2^+ mode is very broad for the formate (about 30 cm^{-1} at RT) compared to the hypophosphite (12.2 cm^{-1}), reflecting disorder in the former case.

Internal vibrations of hypophosphite anion. The free hypophosphite ion has C_{2v} symmetry and 9 fundamental vibrations, i.e., symmetric stretching ($\nu_s(\text{PH}_2)$, A_1), antisymmetric stretching ($\nu_{as}(\text{PH}_2)$, B_1), scissoring ($\delta(\text{PH}_2)$, A_1), rocking ($\rho(\text{PH}_2)$, B_1), twisting ($\tau(\text{PH}_2)$, A_2) and wagging ($\omega(\text{PH}_2)$, B_2) modes of the PH_2 groups as well as symmetric stretching ($\nu_s(\text{PO}_2)$, A_1), antisymmetric stretching ($\nu_{as}(\text{PO}_2)$, B_2) and scissoring ($\delta(\text{PO}_2)$, A_1) modes of the PO_2 moiety [29].

Former experimental and theoretical studies showed that five of the mentioned above vibrations of H_2PO_2^- anion are observed in well-separated regions. That is, $\nu_s(\text{PH}_2)$ at 2345–2424 cm^{-1} , $\nu_{as}(\text{PH}_2)$ at 2305–2368 cm^{-1} , $\tau(\text{PH}_2)$ at 899–945 cm^{-1} , $\rho(\text{PH}_2)$ at 792–834 cm^{-1} and $\delta(\text{PO}_2)$ at 456–518 cm^{-1} [20,30–32]. For $[\text{MHy}][\text{Mn}(\text{H}_2\text{PO}_2)]$, these modes are observed at 2333–2379, 2297–2322, 910–921, 799–824 and 474–519 cm^{-1} , respectively (Table S2).

According to the literature data, the $\nu_{as}(\text{PO}_2)$ and $\delta(\text{PH}_2)$ modes are observed in a similar wavenumber range, typically at 1154–1230 and 1132–1172 cm^{-1} , respectively [20,30–32]. The same behavior is observed for the $\nu_s(\text{PO}_2)$ and $\omega(\text{PH}_2)$ modes that are usually observed at 1024–1062 and 1070–1126 cm^{-1} , respectively [30–32]. Our Raman and IR spectra of $[\text{MHy}][\text{Mn}(\text{H}_2\text{PO}_2)]$ show two separated groups of bands at 1154–1204 and 1048–1092 cm^{-1} . The former bands can be assigned to $\nu_{as}(\text{PO}_2)$ and $\delta(\text{PH}_2)$ modes and the latter to $\nu_s(\text{PO}_2)$ and $\omega(\text{PH}_2)$ ones.

It is worth adding that there are two types of H_2PO_2^- ions in the $[\text{MHy}][\text{Mn}(\text{H}_2\text{PO}_2)]$ structure, one located at site of C_s and second at site of C_1 symmetry [5]. Each fundamental mode of the former (later) anion should split into 4 (8) Davydov components (see Table S3). Indeed, Raman and IR spectra clearly show splitting of each mode into a few bands (Table S2). For instance, two $\tau(\text{PH}_2)$ modes are observed due to two crystallographically distinct H_2PO_2^- ions. Wavenumbers of these modes practically do not depend on polarization, pointing to negligible Davydov splitting. However, the $\nu_s(\text{PH}_2)$, and $\nu_{as}(\text{PH}_2)$ and $\delta(\text{PO}_2)$ split into three components and the $\rho(\text{PH}_2)$ into four components, indicating significant Davydov splitting for these modes.

Lattice modes. Mn^{2+} ions are located in the structure at inversion center and as a result, $\text{T}'(\text{Mn}^{2+})$ mode, are IR-active only (see Table S3). Our IR spectrum shows two strong IR bands at 229 and 280 cm^{-1} that have no Raman counterparts. These bands can be unambiguously assigned to $\text{T}'(\text{Mn}^{2+})$ modes. It is worth noting here that this assignment is consistent with studies of zinc hypophosphites, which revealed $\text{T}'(\text{Zn}^{2+})$ modes at 234–357 cm^{-1} [32].

Modes in the 137–162 cm^{-1} range are much stronger in the IR than Raman spectra while opposite behavior can be noticed for the modes located below 120 cm^{-1} . This behavior is consistent with assignment of the former bands to the coupled modes involving translational motions of $\text{T}'(\text{Mn}^{2+})$ and $\text{T}'(\text{H}_2\text{PO}_2^-)$ ions and the latter ones to librational $\text{L}(\text{H}_2\text{PO}_2^-)$ modes.

3.3. Temperature Dependence of Raman Modes

Raman spectra of the $[\text{MHy}][\text{Mn}(\text{H}_2\text{PO}_2)]$ sample recorded as a function of temperature (80–360 K) are presented in Figure S1. Increasing of temperature leads to broadening and shift of bands. As a consequence, many bands are overlapped and hardly resolved above the room temperature. Since splitting as well as an emergence of additional or a disappearance of already present bands is not observed, the occurrence of a structural phase transition in $[\text{MHy}][\text{Mn}(\text{H}_2\text{PO}_2)]$ can be excluded, in agreement with the literature [5]. This conclusion is further supported by the temperature evolution of wavenumbers and full width at half maximum (FWHM) values for a few selected Raman modes (Figures 4 and 5), which do not show any splitting or departures from the typical anharmonic behavior in the studied temperature range.

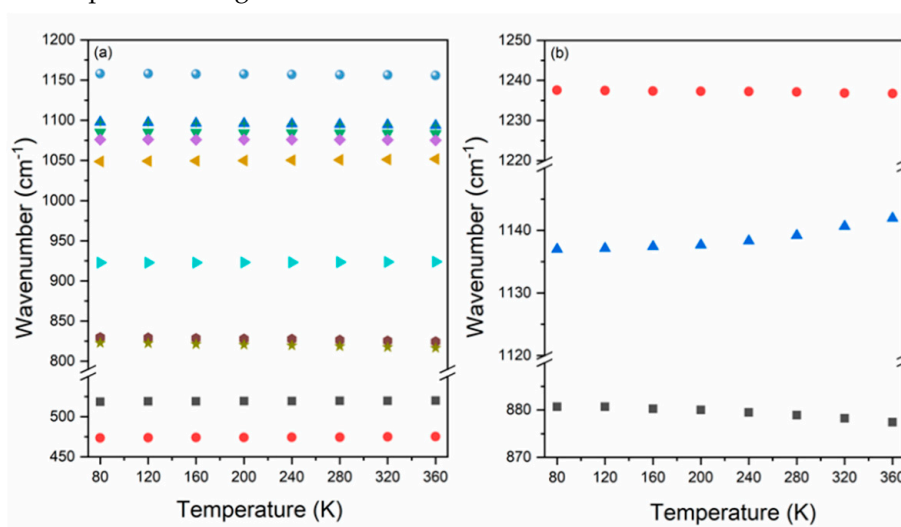


Figure 4. The temperature evolution of Raman wavenumbers of bands corresponding to vibrations of groups that built up (a) H_2PO_2^- and (b) MHy^+ ions.

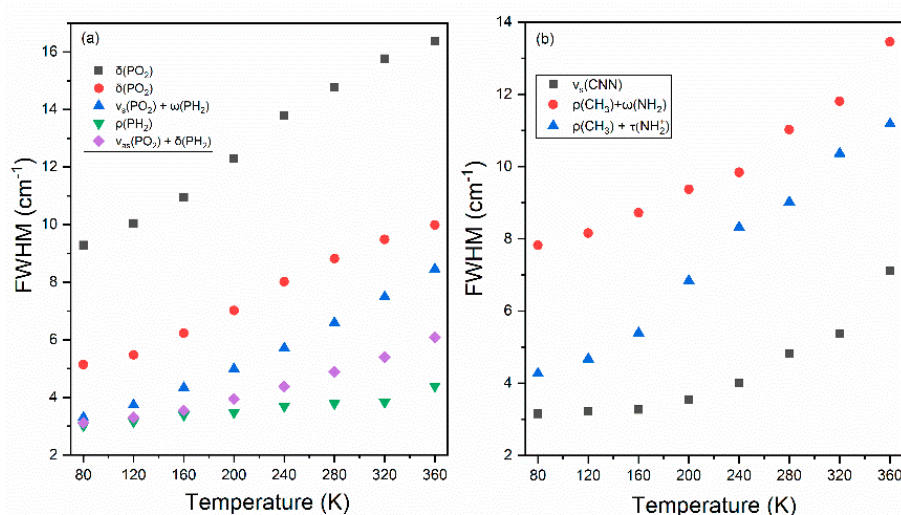


Figure 5. The temperature evolution of Raman full widths at half maximum (FWHMs) of bands corresponding to vibrations of groups that built up (a) H_2PO_2^- and (b) MHy^+ ions.

Figure 4 presents the temperature-dependent evolution of bands assigned to vibrations of PH₂ and PO₂ groups building H₂PO₂⁻ liners. As can be seen, Raman bands exhibit weak hardening upon cooling from 360 K to 80 K, that is, the observed shifts do not exceed 6 cm⁻¹. The largest shift concerns bands located at 823 and 830 cm⁻¹ (360 K) attributed to rocking motions of PH₂ groups (ρPH_2), which upon cooling move toward lowest wavenumbers by about 6 cm⁻¹. Much weaker changes, i.e.,

upshifts by 1 or 2 cm^{-1} , can be observed for bands assigned to bending motions of PO_2 groups (δPO_2) located at 519 and 473 cm^{-1} (at 360 K). Interesting observations can also be made for temperature dependence of FWHM of bands corresponding to vibrations of PH_2 and PO_2 groups (Figure S5a). In this case, modes narrow significantly upon cooling. For instance, the bandwidth of 519 cm^{-1} (RT) Raman band (δPO_2) decreases from 16.4 cm^{-1} (360 K) to 9.3 cm^{-1} (80 K). Much weaker narrowing from 4.4 cm^{-1} (360 K) to 3.0 cm^{-1} (80 K) applies to band located at 822 cm^{-1} (RT), which has the main contribution of the rocking vibration of PH_2 groups. Differences in thermal behavior for different vibrational modes of PH_2 and PO_2 groups can be explained by various surrounding and their different ability to form H-bonding. Please note that two inequivalent H_2PO_2^- units coordinate neighboring Mn^{2+} ions in a different way, and thus the created P-O-Mn angles vary in a broad range (127, 130 and 157°) [5]. These linkers are also involved in the formation of hydrogen bonds (HBs) with the NH_2 groups from MHy^+ cations, which is directly responsible for the off-center displacement of organic ions inside the cavities. Decrease of temperature leads to slowing down of thermally-activated motions followed by decrease of the unit cell volume and increase of the HBs strength. Since the impact of HBs is not the same for the PH_2 and PO_2 groups, different thermal behavior for modes attributed to their vibrations can be observed.

Similar behavior also applies to bands assigned to vibrational motions of MHy^+ cations (Figure 4b). In this case, the observed shifts do not exceed 5 cm^{-1} . The largest changes are observed for bands at 1142 cm^{-1} and 881 cm^{-1} (360 K). Upon cooling, the first peak corresponding to mixed rocking and torsion vibrations of the NH_2 groups exhibits downshift to 1137 cm^{-1} , whereas the second one originating from symmetric stretching vibrations of the CNN moieties changes its position to 877 cm^{-1} . Meanwhile, minimal hardening of 0.8 cm^{-1} upon cooling is noticed for the band at 1237 cm^{-1} (RT) attributed to mixed rocking vibrations of the CH_3 groups and wagging motions of the NH_2 groups. As in the case of vibrations of H_2PO_2^- linkers, observed differences in thermal evolution of modes attributed to vibrational motions of MHy^+ ions can also be explained by different influence of HBs on particular groups in the structure.

The thermal behavior of FWHM of the 878 cm^{-1} (RT), 1237 cm^{-1} and 1139 cm^{-1} bands corresponding to the $\nu_s\text{CNN}$, $\rho\text{CH}_3+\omega\text{NH}_2$ and $\rho\text{CH}_3+\tau\text{NH}_2^+$ modes, respectively, is presented at Figure 5b. As can be seen, upon cooling all mentioned bands exhibit significant narrowing. The larger narrowing, by almost 9 cm^{-1} , is observed for the band attributed to mixed rocking vibration of the CH_3 groups and twisting vibrations of the NH_2^+ groups. Observed results prove that change of temperature leads to strong change in the HB strengths.

4. Conclusions

Phonon properties of manganese hypophosphite framework templated by methylhydrazinium cations were studied using IR and Raman spectroscopies. We have presented selection rules for the *Pnma* orthorhombic phase together with proposed assignment of the observed IR and Raman bands to the respective internal and lattice vibrations. Presented ascription was based on our DFT calculations made for the isolated MHy^+ ion in harmonic and anharmonic approximations. Polarized Raman spectra provided additional information on magnitude of Davydov splitting observed in the studied organic-inorganic hybrid. The temperature-dependent Raman studies allowed us to obtain deeper insight into structural changes occurring in the $[\text{MHy}][\text{Mn}(\text{H}_2\text{POO})_3]$ compound. Differences in the temperature evolution of wavenumbers and FWHMs of bands attributed to vibrational motions of the MHy^+ as well as H_2PO_2^- ions can be explained by the different influence of HB on individual groups that built this structure.

Supplementary Materials: The following are available online, Figure S1: The temperature-dependent Raman spectra, Table S1: Selected bond lengths and bond angles of MHy^+ cation. Table S2: Raman and IR wavenumbers of $[\text{MHy}][\text{Mn}(\text{H}_2\text{POO})_3]$ at RT, Table S3: The correlation diagram and irreducible representations for the *Pnma* orthorhombic phase of the $[\text{MHy}][\text{Mn}(\text{H}_2\text{POO})_3]$ crystal.

Author Contributions: Conceptualization, A.C.-L., M.P. and M.M.; data curation, M.M.; formal analysis, J.H.; funding acquisition, M.M.; investigation, A.C.-L. and M.P.; methodology, M.P.; project administration, M.M.; resources, M.M.; software, E.K.; supervision, M.M.; validation, A.C.-L., M.P. and M.M.; visualization, A.C.-L.; writing—original draft, A.C.-L., M.P., E.K. and M.M.; writing—review and editing, M.M. All authors have read and agreed to the published version of the manuscript.

Funding: This research was funded by National Science Center (Narodowe Centrum Nauki) in Poland, grant number 2018/31/B/ST5/00455.

Conflicts of Interest: The authors declare no conflict of interest.

References

1. Wang, F.; Cao, Y.; Chen, C.; Chen, Q.; Wu, X.; Li, X.; Qin, T.; Huang, W. Materials Toward the Upscaling of Perovskite Solar Cells: Progress, Challenges, and Strategies. *Adv. Funct. Mater.* **2018**, *28*, 1803753. [[CrossRef](#)]
2. Zhao, X.; Ng, J.D.A.; Friend, R.H.; Tan, Z.-K. Opportunities and Challenges in Perovskite Light-Emitting Devices. *ACS Photonics* **2018**, *5*, 3866–3875. [[CrossRef](#)]
3. Maćzka, M.; Ptak, M.; Gaĝor, A.; Stefańska, D.; Sieradzki, A. Layered Lead Iodide of [Methylhydrazinium]₂PbI₄ with a Reduced Band Gap: Thermochromic Luminescence and Switchable Dielectric Properties Triggered by Structural Phase Transitions. *Chem. Mater.* **2019**, *31*, 8563–8575. [[CrossRef](#)]
4. Maćzka, M.; Stefańska, D.; Zareba, J.K.; Nyk, M.; Sieradzki, A. Temperature-dependent luminescence and second-harmonic generation of perovskite-type manganese and cadmium dicyanamide frameworks templated by tetrapropylammonium cations. *J. Alloys Compd.* **2020**, *821*, 153464. [[CrossRef](#)]
5. Maćzka, M.; Gaĝor, A.; Pikul, A.; Stefańska, D. Novel hypophosphite hybrid perovskites of [CH₃NH₂NH₂][Mn(H₂POO)₃] and [CH₃NH₂NH₂][Mn(H₂POO)_{2.83}(HCOO)_{0.17}] exhibiting antiferromagnetic order and red photoluminescence. *RSC Adv.* **2020**, *10*, 19020–19026. [[CrossRef](#)]
6. Jain, P.; Ramachandran, V.; Clark, R.J.; Zhou, H.D.; Toby, B.H.; Dalal, N.S.; Kroto, H.W.; Cheetham, A.K. Multiferroic behavior associated with an order-disorder hydrogen bonding transition in metal-organic frameworks (MOFs) with the perovskite ABX₃ architecture. *J. Am. Chem. Soc.* **2009**, *131*, 13625–13627. [[CrossRef](#)]
7. Tian, Y.; Stroppa, A.; Chai, Y.; Yan, L.; Wang, S.; Barone, P.; Picozzi, S.; Sun, Y. Cross coupling between electric and magnetic orders in a multiferroic metal-organic framework. *Sci. Rep.* **2015**, *4*, 6062. [[CrossRef](#)]
8. Maćzka, M.; Gaĝor, A.; Ptak, M.; Paraguassu, W.; Da Silva, T.A.; Sieradzki, A.; Pikul, A. Phase transitions and coexistence of magnetic and electric orders in the methylhydrazinium metal formate frameworks. *Chem. Mater.* **2017**, *29*, 2264–2275. [[CrossRef](#)]
9. Bermúdez-García, J.M.; Sánchez-Andújar, M.; Castro-García, S.; López-Beceiro, J.; Artiaga, R.; Señaris-Rodríguez, M.A. Giant barocaloric effect in the ferroic organic-inorganic hybrid [TPrA][Mn(dca)]₃ perovskite under easily accessible pressures. *Nat. Commun.* **2017**, *8*, 15715. [[CrossRef](#)]
10. Maćzka, M.; Gaĝor, A.; Ptak, M.; Stefańska, D.; Macalik, L.; Pikul, A.; Sieradzki, A. Structural, phonon, magnetic and optical properties of novel perovskite-like frameworks of TriBuMe[M(dca)₃] (TriBuMe = tributylmethylammonium; dca = dicyanamide; M = Mn²⁺, Fe²⁺, Co²⁺, Ni²⁺). *Dalton Trans.* **2019**, *48*, 13006–13016. [[CrossRef](#)]
11. Geng, F.-J.; Zhou, L.; Shi, P.-P.; Wang, X.-L.; Zheng, X.; Zhang, Y.; Fu, D.-W.; Ye, Q. Perovskite-type organic-inorganic hybrid NLO switches tuned by guest cations. *J. Mater. Chem. C* **2017**, *5*, 1529–1536. [[CrossRef](#)]
12. Maćzka, M.; Ptak, M.; Gaĝor, A.; Stefańska, D.; Zareba, J.K.; Sieradzki, A. Methylhydrazinium Lead Bromide: Noncentrosymmetric Three-Dimensional Perovskite with Exceptionally Large Framework Distortion and Green Photoluminescence. *Chem. Mater.* **2020**, *32*, 1667–1673. [[CrossRef](#)]
13. Maćzka, M.; Gaĝor, A.; Zareba, J.K.; Stefańska, D.; Drozd, M.; Balciunas, S.; Šimenas, M.; Banys, J.; Sieradzki, A. Three-Dimensional Perovskite Methylhydrazinium Lead Chloride with Two Polar Phases and Unusual Second-Harmonic Generation Bistability above Room Temperature. *Chem. Mater.* **2020**, *32*, 4072–4082. [[CrossRef](#)]
14. Maćzka, M.; Collings, I.E.; Furtado Leite, F.; Paraguassu, W. Raman and single-crystal X-ray diffraction evidence of pressure-induced phase transitions in a perovskite-like framework of [(C₃H₇)₄N][Mn(N(CN)₂)₃]. *Dalton Trans.* **2019**, *48*, 9072–9078. [[CrossRef](#)]
15. Maćzka, M.; Ptak, M.; Gaĝor, A.; Sieradzki, A.; Peksa, P.; Usevicius, G.; Simenas, M.; Leite, F.F.; Paraguassu, W. Temperature- and pressure-dependent studies of a highly flexible and compressible perovskite-like cadmium dicyanamide framework templated with protonated tetrapropylamine. *J. Mater. Chem. C* **2019**, *7*, 2408–2420. [[CrossRef](#)]

16. Wu, Y.; Shaker, S.; Brivio, F.; Murugavel, R.; Bristowe, P.D.; Cheetham, A.K. [Am]Mn(H₂POO)₃: A new family of hybrid perovskites based on the hypophosphite ligand. *J. Am. Chem. Soc.* **2017**, *139*, 16999–17002. [CrossRef]
17. Gao, H.-Q.; Wei, W.-J.; Tan, Y.-H.; Tan, Y.-Z. Phase Transition and negative Thermal Expansion in Guanidinium Magnesium-Hypophosphite Hybrid Perovskite. *Chem. Mater.* **2020**, *32*, 6886–6891. [CrossRef]
18. Wu, Y.; Halat, D.M.; Wei, F.; Binford, T.; Seymour, I.D.; Gaultois, M.W.; Shaker, S.; Wang, J.; Grey, C.P.; Cheetham, A.K. Mixed X-site formate-hypophosphite hybrid perovskites. *Chem. A Eur. J.* **2018**, *24*, 11309–11313. [CrossRef]
19. Wu, Y.; Binford, T.; Hill, J.A.; Shaker, S.; Wang, J.; Cheetham, A.K. Hypophosphite hybrid perovskites: A platform for unconventional tilts and shifts. *Chem. Commun.* **2018**, *54*, 3751–3754. [CrossRef]
20. Ptak, M.; Maćzka, M. Phonon properties and mechanism of order-disorder phase transition in formamidinium manganese hypophosphite single crystal. *Spectrochim. Acta A* **2020**, *230*, 118010. [CrossRef]
21. Frisch, M.J.; Trucks, G.W.; Schlegel, H.B.; Scuseria, G.E.; Robb, M.A.; Cheeseman, J.R.; Montgomery, J.A., Jr.; Vreven, T.; Kudin, K.N.; Burant, J.C.; et al. *Gaussian 03, Revision A.1*; Gaussian, Inc.: Pittsburgh, PA, USA, 2003.
22. Becke, D. Density-functional thermochemistry. IV. A new dynamical correlation functional and implications for exact-exchange mixing. *J. Chem. Phys.* **1996**, *104*, 1040–1046. [CrossRef]
23. Lee, C.; Yang, W.; Parr, R.G. Development of the Colle-Salvetti correlation-energy formula into a functional of the electron density. *Phys. Rev. B* **1988**, *37*, 785–789. [CrossRef]
24. Parr, R.G.; Yang, W. *Density-Functional Theory of Atoms and Molecules*; Oxford University Press: New York, NY, USA, 1989.
25. McLean, A.D.; Chandler, G.S. Contracted Gaussian basis sets for molecular calculations. I. Second row atoms, $Z = 11$ –18. *J. Chem. Phys.* **1980**, *72*, 5639–5648. [CrossRef]
26. Krishnan, R.; Binkley, J.S.; Seeger, R.; Pople, J.A. Self-consistent molecular orbital methods. XX. A basis set for correlated wave functions. *J. Chem. Phys.* **1980**, *72*, 650–654. [CrossRef]
27. Zhurko, G.A.; Zhurko, D.A. Chemcraft Graphical Program of Visualization of Computed Results. Available online: <http://chemcraftprog.com> (accessed on 6 July 2020).
28. Rostkowska, H.; Lapinski, L.; Nowak, M.J. Analysis of the normal modes of molecules with D_{3h} symmetry. Infrared spectra of monomeric s-triazine and cyanuric acid. *Vib. Spectrosc.* **2009**, *49*, 43–51. [CrossRef]
29. Tabacik, V.; Abenoza, M. Quasi general harmonic force field and mode anharmonicity of the hypophosphite ion normal vibrations. *J. Mol. Struct.* **1975**, *27*, 369–381. [CrossRef]
30. Tsuboi, M. Vibrational Spectra of Phosphite and hypophosphite anions, and the characteristic frequencies of PO₃[−] and PO₂[−] groups. *J. Am. Chem. Soc.* **1957**, *79*, 1351–1354. [CrossRef]
31. Liu, R.; Moody, P.R.; Vanburen, A.S.; Clark, J.A.; Crauser, J.A.; Tate, D.R. On assignment of fundamental vibrational modes of hypophosphite anion and its deuterated analogue. *Vib. Spectrosc.* **1996**, *10*, 325–329. [CrossRef]
32. Tanner, P.A.; Yu-Long, L.; Mak, T.C.W. Synthesis, crystal structures and vibrational spectra of zinc hypophosphites. *Polyhedron* **1997**, *16*, 495–505. [CrossRef]

Sample Availability: Samples of the compound ([CH₃NH₂NH₂][Mn(H₂PO₂)₃] is available from the authors.

Publisher's Note: MDPI stays neutral with regard to jurisdictional claims in published maps and institutional affiliations.



© 2020 by the authors. Licensee MDPI, Basel, Switzerland. This article is an open access article distributed under the terms and conditions of the Creative Commons Attribution (CC BY) license (<http://creativecommons.org/licenses/by/4.0/>).